Synthesis and Characterization of Highly Ordered Co−MCM-41 for Production of Aligned Single Walled Carbon Nanotubes (SWNT)

Sangyun Lim,[†] Dragos Ciuparu,[†] Chanho Pak,[‡] Frank Dobek,[§] Yuan Chen,[†] David Harding,[§] Lisa Pfefferle,[†] and Gary Haller*[,†]

Department of Chemical Engineering, Yale University, New Haven, Connecticut 06520, Materials and Devices Laboratory, Samsung Advanced Institute of Technology, Suwon, Korea, and University of New Haven, West Haven, Connecticut 06516

Received: April 17, 2003; In Final Form: July 30, 2003

Highly ordered cobalt substituted MCM-41 samples were synthesized and characterized for application as catalytic templates for producing aligned single walled carbon nanotubes (SWNT). Highly reproducible Co−MCM-41 samples were successfully synthesized using alkyl templates with 10, 12, 14, 16, and 18 carbon chain lengths by direct incorporation of cobalt into the siliceous MCM-41 framework using a hydrothermal method; the pore size and the pore volume can be controlled precisely. The local environment of cobalt as determined by UV−vis spectroscopy is a mixture of tetrahedral and distorted tetrahedral structures similar to those observed in Co_3O_4. Cobalt atoms are uniformly distributed in the pores (about 30−40/pore) at nearly atomic dispersion probed by XAFS. Incorporation of cobalt into siliceous MCM-41 improves the structure, most likely by dehydroxylation and/or knitting the defective structure of the amorphous silica polymer. The optimum crystallization temperature and time were 100 °C and 4 days for siliceous MCM-41 and 6 days for Co−MCM-41, respectively. Co−MCM-41 is very stable against reducing and oxidation conditions at temperatures under 750 °C. The catalytic templates showed over 90% selectivity to SWNT with up to 4 wt % carbon yield. The growth of SWNT in the pores of Co−MCM-41 was confirmed by Raman spectroscopy and TEM. The catalytic template maintained its structure after successive reaction cycles, which suggests that Co−MCM-41 is a very stable template for producing SWNT under harsh reaction conditions.

Introduction

Single-walled carbon nanotubes (SWNT) exhibit exceptional chemical and physical properties that have suggested a vast number of potential applications.[1] A wide range of device applications require the use of aligned carbon nanotubes of uniform electronic properties. Catalytic synthesis is known to be one of the most effective ways to control the selectivity to SWNT with high yield, and it has the potential to be scaled-up at relatively low cost.[2,3] Among the investigated catalysts, a cobalt and molybdenum impregnated silica catalyst has shown excellent SWNT yield and selectivity.[2] Most methods, however, have a major disadvantage because they produce random sized SWNT requiring tedious postsynthesis separation and alignment of SWNT having homogeneous electronic properties for the desired application. This major impediment may be solved by growth of SWNT inside the pores of a catalytic template with a parallel pore system of uniform size.

The possibility of growing SWNT in the pores of a template catalyst (ALPO-5) was recently reported.[4] This zeolite has an upper limit in channel size of 0.73 nm. An intriguing finding from this zeolite work is that interactions with the channel walls during nanotube formation were observed to lead to selection of a particular nanotube form.[5,6] In general, zeolites are limited to micropores (less than 1.5 nm in diameter) and the channel size cannot be varied without changing the structure and the chemical composition of the final material, which makes zeolites inappropriate for the controlled templated growth of SWNT. In contrast with zeolites, MCM-41 has thin walls of amorphous silica allowing the pore size to be varied from 2 to 10 nm, and chemical properties can be manipulated. This is the ideal template material, allowing independent control of both composition and channel size and, thus, has potential for selective growth of specific forms of metallic or semiconducting SWNTs. There has been demonstration of nanotube growth on/in an MCM-41 like material with an impregnated Fe catalyst.[7] Although this work demonstrated the feasibility of the idea, it did not make use of the most interesting features made possible by the MCM-41 material, namely the incorporation of the metal into the framework at a specified pore size, thus enabling control of the type of nanotube grown. Also, incorporation of the catalytic component in the framework has important implications for selectivity as it may stabilize the metal from reduction or sintering, a necessary condition according to Herrera et al.[2]

We report here on the results of our first attempt of templated growth of SWNT. We chose MCM-41 as a template material and incorporated cobalt as a catalytic active component in the silica framework, resulting in isolated cobalt ions in the pore walls. Co−MCM-41 samples synthesized under various conditions were thoroughly investigated by various characterization techniques such as nitrogen physisorption, XRD, TEM, diffuse reflectance (DR), UV−vis spectroscopy, and X-ray absorption. This made it possible to determine the chemical and structural properties of catalytic template material used for the synthesis of SWNTs.

[†] Yale University.
[‡] Samsung Advanced Institute of Technology.
[§] University of New Haven.

10.1021/jp0304778 CCC: $25.00
Published on Web 09/11/2003

Experimental Section

Materials. Silica synthesis sources used were HiSil-915 from Pittsburgh Plate Glass (PPG) and tetramethylammonium silicate (10 wt % silica, SACHEM Inc.). The Co source was $CoSO_4 \cdot xH_2O$ (Aldrich Chemical Co.). The quaternary ammonium surfactants $C_nH_{2n+1}(CH_3)_3NBr$ were purchased from Aldrich Chemical Co. with $n = 12, 14, 16, 18$ and from American Tokyo Kasei with $n = 10$. The surfactant solutions were prepared by ion-exchanging the 29 wt % (C10 and C12), 20 wt % (C14 and C16), and 10 wt % (C18) $C_nH_{2n+1}(CH_3)_3NBr$ aqueous solutions with equal molar exchange capacity of Amberjet-400 (OH) ion-exchange resin (Sigma Chemical Co.) by overnight batch mixing. The antifoaming agent was Antifoam A from Sigma Chemical Co., a silane polymer alkyl terminated by methoxy groups. Acetic acid (Fisher Scientific) was used for pH adjustment of the synthesis solution. In the text hereafter specific samples are designated by the alkyl chain length of the surfactant used (e.g., C10 Co−MCM-41).

Synthesis. HiSil-915, tetramethylammonium silicate and the Co aqueous solution were mixed for 30 min. The water to total silica ratio was varied from 74.4 to 86.0 mole ratio based on the surfactant chain length. The surfactant solution was added to the prepared silica and Co mixture and a small amount of antifoaming agent (0.2 wt % of surfactant) was incorporated to remove excess foam produced by the surfactant as a result of stirring the synthesis solution. Acetic acid was added until pH = 11 was reached. After additional mixing for about 10 min, this synthesis solution was poured into a polypropylene bottle and placed in the autoclave at 100 or 150 °C for 6 days. After cooling to room temperature, the resulting solid was recovered by filtration, washed with deionized water and dried under ambient conditions. The predried solid was heated from room temperature to 540 °C for 20 h under He (30 mL/min) and soaked for 1 h at 540 °C in flowing He followed by 6 h of calcination at 540 °C under flowing air to remove the residual organics. The molar ratio of each component in the synthesis solution was controlled at SiO_2: surfactant:Co:H_2O = 1:0.27:0.01:X (X = 74.4−86.0). Because the preparation process may cause some loss of Co and silica in the byproducts, the final Co content of each sample was determined by ICP at Galbraith Laboratories, Inc. A pure siliceous MCM-41 was also prepared following the procedure described above for Co−MCM-41, without incorporating the cobalt into the synthesis solution.

Characterizations. *N_2 Physisorption.* Nitrogen adsorption−desorption isotherms were measured at −196 °C with a static volumetric instrument Autosorb-1C (Quanta Chrome). Prior to the measurement, the samples were outgassed at 200 °C to a residual pressure below 1×10^{-4} Torr. A Baratron pressure transducer (0.001−10 Torr) was used for low-pressure measurements. The pore size distributions were calculated from the desorption isotherms using the BJH method.[8] Ravikovitch et al.[9] reported that pore diameter values determined using the BJH method are underestimated, and the nonlocal density functional theory (NLDFT) is more reliable for the mesopore size prediction. However, the pore size distribution determined in our study by the BJH method provides reliable results that can be used for the relative comparison of the synthesized samples. Other complementary techniques such as HR-TEM were also used to confirm the structure and the pore size.

XRD. X-ray diffraction measurements were carried out using a Shimadzu X-ray diffractometer (Cu Kα, λ = 0.154 nm, 40 kV, 30 mA) to check if the prepared Co−MCM-41 has the characteristic hexagonal pore structure after calcination and reaction. The pore wall thickness was calculated from the XRD relationship between the lattice parameter and the spacing. ($a_o = 2d_{100}/\sqrt{3}$) and N_2 physisorption results for pore diameter determination. The wall thickness was estimated to be 1 nm, independent of the pore diameter.

DR UV−vis. The UV−vis spectra were recorded by diffuse reflectance on a Hewlett-Packard 8452A diode array spectrometer equipped with a Harrick praying mantis. All spectra were recorded at room temperature under ambient atmosphere. Samples consisting of 100 mg of powder were pressed in the sample holder by hand to make a thick wafer. The reference samples were diluted to 1 wt % with siliceous MCM-41.The final spectra of cobalt were obtained by subtracting the spectra of the pure siliceous MCM-41.

X-ray Absorption. X-ray absorption measurement was performed at the Co K edge (7709 eV) using Si (111) as the monochromator crystal at station X23A2 in NSLS, 2.5 GeV storage ring, Brookhaven National Laboratory. Samples were pressed into self-supporting wafers and placed in a stainless steel cell equipped with water-cooled Kapton windows, a gas inlet and outlet, and a heating unit allowing in situ gas treatment. Details on the experimental procedure are given elsewhere.[10]

Raman Spectroscopy. Raman spectra were recorded on a LabRam instrument from Jobin Yvon Horiba equipped with an Olympus confocal microscope using an excitation wavelength of 532 nm.

Results and Discussion

Fresh Co−MCM-41 Samples (before Reaction). Figure 1 shows the nitrogen physisorption results of C10 to C18 Co−MCM-41 samples. In this study, nitrogen physisorption was used as a standard method to compare the structure of each sample because it shows the volume averaged value, unlike XRD or TEM, which only probe a limited part of the samples. The full width at half-maximum (fwhm) of the pore size distribution (PSD) curve and the slope of the capillary condensation in the isotherms were determined for each sample and used as structure indexes for comparisons. Figure 1a shows the isotherms of C10 to C18 Co−MCM-41 samples. All samples show capillary condensation, suggesting the Co−MCM-41 samples were successfully synthesized regardless of the surfactant chain length. As is well-known, the longer surfactant chain length results in the higher relative pressure of the capillary condensation. When the pore size distribution for each sample was compared, the pore size increased systematically and the corresponding pore volume varied linearly with the surfactant chain length. This implies that the pore size and the pore volume can be precisely controlled using the synthesis method described in this study. The mesopore volume, defined in this study as the volume of pores with diameters below 10 nm, shows a linear dependence on the surfactant chain length (see Figure 2). This control shows potential for controlling the size and the amount of carbon nanotubes produced in the pore system of these catalytic template materials. The slope of capillary condensation and the fwhm used as structure indexes are listed in Table 1. Longer surfactant chain lengths result in narrower fwhms and steeper slopes for the capillary condensation. These results are highly reproducible with most of the transition metal incorporated MCM-41 samples prepared following the method described in the Experimental Section. Modeling work aimed at predicting the sample structure and metal loading is under development for V−MCM-41,[11] and it will be extended to Co−MCM-41 soon.

The sample synthesized using the C18 surfactant shows a broader fwhm than those of Co−MCM-41 samples synthesized

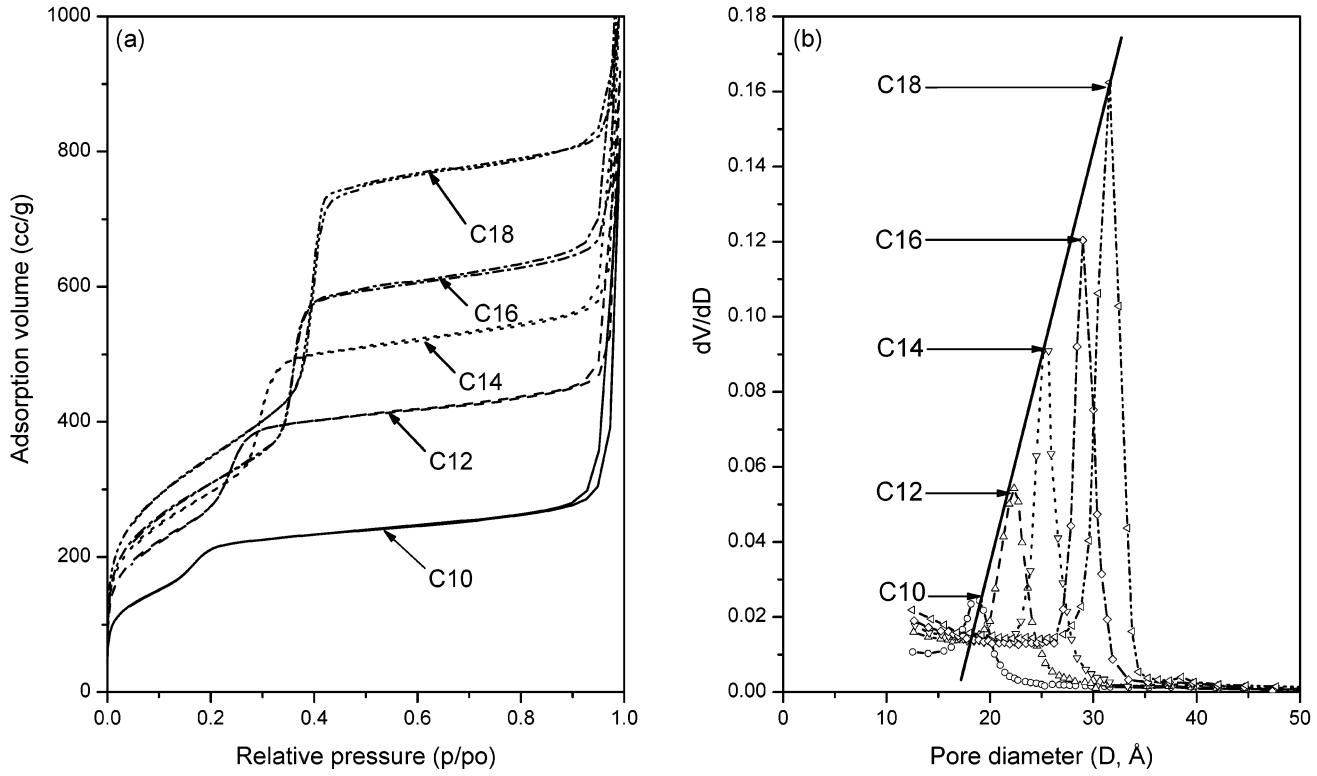

Figure 1. Nitrogen physisorption results of C10−C18 Co−MCM-41 samples: (a) adsorption/desorption isotherms; (b) pore size distributions.

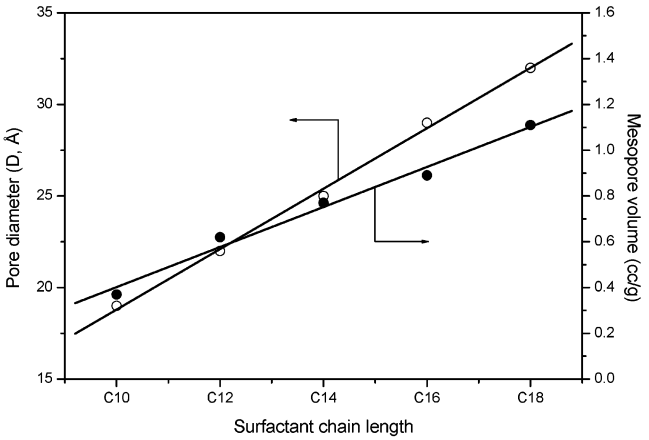

Figure 2. Relationship between surfactant chain length, pore diameter, and mesopore volume.

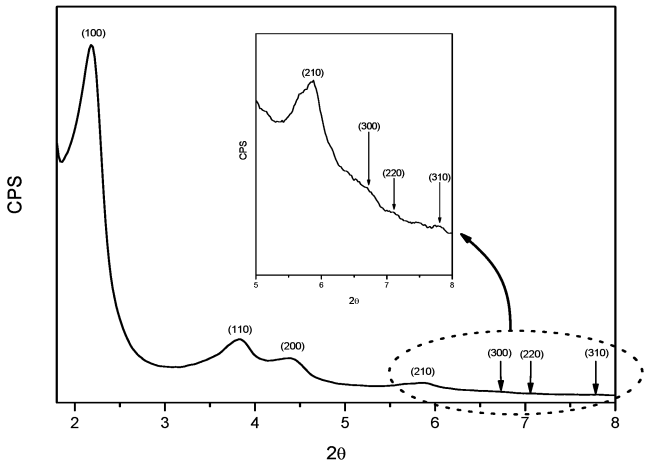

Figure 3. XRD pattern of C16 Co−MCM-41.

TABLE 1: Full Width at Half-Maximum (fwhm) and the Maximum Slope of the Capillary Condensation for C10−C18 Co−MCM-41 Samples

catalysts	metal loading[a] (wt %)	fwhm (Å)	max. slope[b] (cc/g)
C10 Co−MCM-41	1	3.94	844
C12 Co−MCM-41	1	3.14	1980
C14 Co−MCM-41	1	2.23	3637
C16 Co−MCM-41	1	2.16	5463
C18 Co−MCM-41	1	2.58	8077

[a] Initial metal loading in the synthesis solution. [b] Maximum slope of capillary condensation of the isotherm.

using C16 and C14 surfactants, which may be attributed to the partially undissolved C18 surfactant in the synthesis solution. However, the slope, also considered as a structure index, shows the highest value because the maximum slope is controlled by dissolved surfactant only.

All samples (C10−C18) were characterized by XRD to confirm the MCM-41 structure. A typical XRD pattern is illustrated in Figure 3 for C16 Co−MCM-41. As expected from the nitrogen physisorption results, the MCM-41 structure is extremely well ordered. When recorded with a regular powder X-ray diffractometer, the XRD pattern of a well ordered MCM-41 sample usually shows one main peak (100) and three other small peaks (110, 200, and 210). If the diffraction pattern is recorded using a high-energy X-ray beam (synchrotron), the well ordered MCM-41 sample shows several additional peaks (300, 220, and 310). We observed seven diffraction lines with our sample using a regular powder X-ray diffractometer, showing that the samples synthesized by this method have an outstanding regularity of the structure. This result confirms the reliability of our recipe for the synthesis of mesoporous molecular sieves.

Figure 4 shows the nitrogen physisorption results of the C16 pure siliceous and Co−MCM-41 with 0.66 wt % of Co. Both

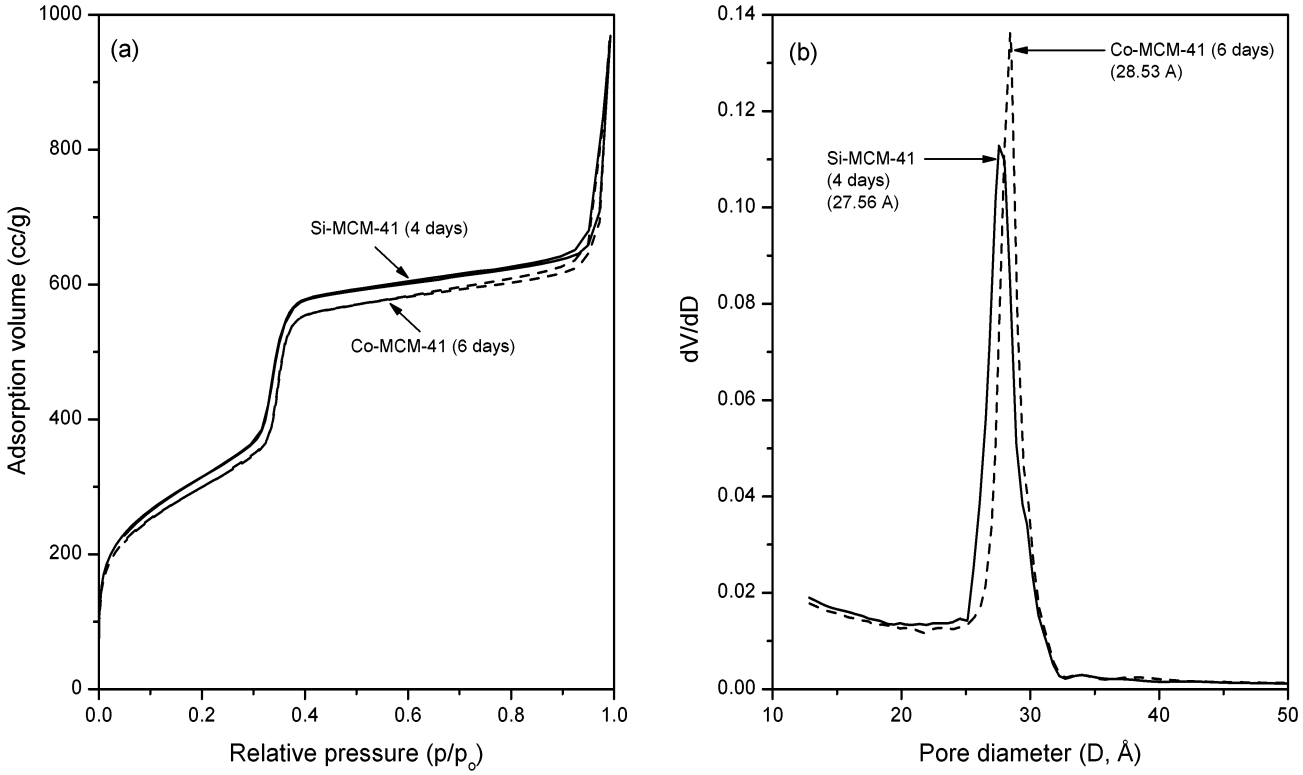

Figure 4. Nitrogen physisorption results of siliceous and Co−MCM-41 samples: (a) adsorption/desorption isotherms; (b) pore size distributions.

samples show almost identical isotherms and pore size distribution curves. However, the incorporation of cobalt increases the pore size about 0.1 nm compared to siliceous MCM-41. This may be due to the differences in the bond lengths between the cations and oxygen. The Co−O bond length is longer than that of Si−O. On the basis of this rationale the increase of pore size suggests that cobalt is incorporated in the silica framework so that the longer Co−O bond leads to an increase of the pore size. Temperature programmed reduction (TPR) was performed for these samples as a complementary experiment, and no surface cobalt oxide was observed (not shown). It has been demonstrated that when cobalt exists on the surface of silica, the multiple silanol bonds to a cobalt atom contract the pore wall, which results in the decrease of the pore size.[12] These results suggest that cobalt was successfully incorporated into the silica framework.

To investigate the local environment of cobalt in the MCM-41 material, samples were analyzed by DR UV−vis spectroscopy and X-ray absorption near edge structure (XANES). The Co−MCM-41 samples show three different groups of peaks in the UV−vis region, as shown in Figure 5. Cobalt aluminate ($CoAl_2O_4$) and Co_3O_4 were selected as reference samples for comparison. The spectra of $CoAl_2O_4$ shows a transition in the 550−700 nm range, characteristic for tetrahedrally coordinated Co^{2+}.[13] The Co_3O_4 is a mixed oxide with the cobalt in both tetrahedral and octahedral coordinations that absorb energy around 300−400 nm.[14] All of the Co−MCM-41 samples show three major groups of peaks, which result from oxygen to metal charge transfer at 247 nm,[15] mixed oxide of cobalt at 340 and 385 nm, and tetrahedrally coordinated Co^{2+} in the silica framework at 580, 650, and 684 nm. These interpretations are exactly coincident with the reference samples (Co_3O_4 and $CoAl_2O_4$). However, the features between 300 and 400 nm can be assigned to Co^{3+} in a distorted tetrahedral environment,[16,17] or to a portion of the Co species outside the framework.[18] As we could not find any evidence of octahedrally coordinated,

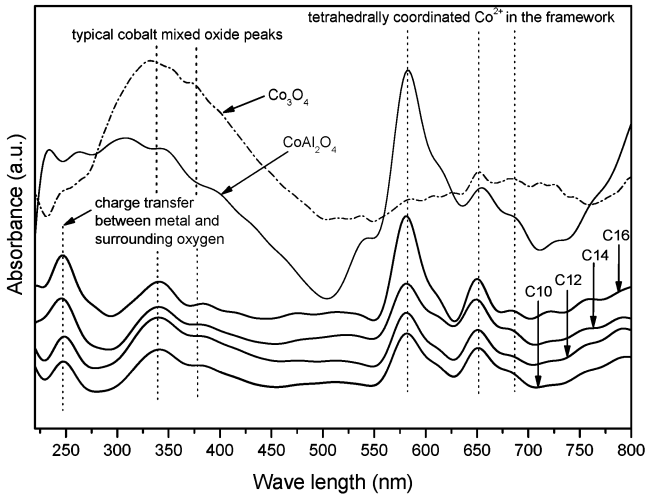

Figure 5. DR UV−vis spectra of C10−C16 Co−MCM-41 and reference samples.

extraframework cobalt on the surface, complete incorporation of cobalt in the silica framework is likely, and these peaks can only be assigned to distorted tetrahedral Co^{3+}.

Figure 6 illustrates the XANES results of a C16 Co−MCM-41 sample compared to the reference samples. It shows that the sample synthesized here has a pre-edge peak close to that of Co_3O_4. This suggests that the cobalt species in MCM-41 consist of a mixture of tetrahedral and octahedral local structures such as Co_3O_4. As discussed in the UV−vis section, it may be a mixture of tetrahedral and distorted tetrahedral coordination of Co^{2+} and Co^{3+}, respectively, with a pseudo-octahedral environment attained at some sites due to hydration. Several studies reporting tetrahedral coordination for cobalt in Co_3O_4 made this interpretation more reliable.[13] Co^{3+} can be formed by calcination of the as-synthesized Co−MCM-41. We could see the shift of the absorbance peaks in the UV−vis spectra to

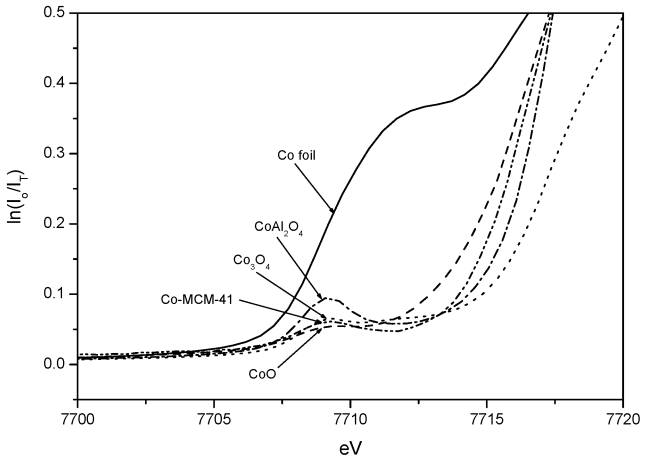

Figure 6. XANES spectra of C16 Co−MCM-41 and reference samples.

TABLE 2: Chemical Analysis (by ICP) Results of C10−C16 Co−MCM-41 Samples

sample	analysis	wt %
C10 Co−MCM-41	cobalt	0.68
C12 Co−MCM-41	cobalt	0.68
C14 Co−MCM-41	cobalt	0.66
C16 Co−MCM-41	cobalt	0.66

higher wavelengths after the sample was calcined at higher temperatures (not shown).

All the samples used for nanotube growth in this study were synthesized on the basis of the initial concentration of 1 wt % Co. There is some loss of cobalt during sample synthesis. The actual cobalt amounts in MCM-41 determined by ICP analysis are given in Table 2. Each sample contains between 0.66 and 0.68 wt % of cobalt, regardless of the surfactant chain length. The number of cobalt atoms per pore was calculated using eq 1 with the assumptions as follows: (1) straight cylindrical pore of 100 nm length (by TEM and refs 19 and 20), (2) wall thickness of 1 nm (by XRD, N_2 physisorption, and TEM), (3) constant wall density that is equal to amorphous silica.

$$N_{Co} = {}^1/_2\pi[(\text{O.D.}/2)^2 - (\text{I.D.}/2)^2]L\rho MA_N \qquad (1)$$

where N_{Co} is number of cobalt atoms per pore, O.D. is the outside diameter of a pore, I.D. is the inside diameter of a pore, L is the pore length (100 nm), ρ is the density of silica (2.2 g/cm^3), M is the total number of moles of cobalt atoms per unit mass (mol/g), and A_N is Avogadro's number.

As shown in Figure 7, increasing pore diameter results in the linear increase of the number of cobalt atoms in the pore. The difference is 3−4 atoms between different pore sizes, which may result in the precise control of metal particle size by reduction for the synthesis of single walled carbon nanotubes.

To determine how much cobalt can be incorporated in the silica framework, a series of Co−MCM-41 samples (0.1−5 wt % Co−MCM-41) were synthesized and characterized by nitrogen physisorption. As observed previously, up to a certain amount of metal, incorporation of cobalt improves the structure of MCM-41 by knitting the defective amorphous structure of the silica polymer,[21] which results in a pore size increase while unimodal pore size distribution is maintained. The knitting effect of cobalt starts from 1 wt % (initial concentration) as shown in Figure 8. This suggests that a cobalt content below 1 wt % (actual concentration is 0.66 wt %) is not enough to affect the structure. It is notable that there is a large jump in the pore size

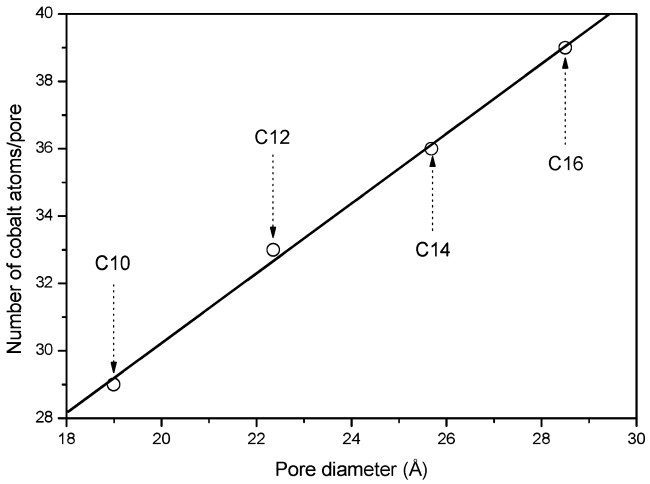

Figure 7. Variation of the calculated number of cobalt atoms and surfactant chain length.

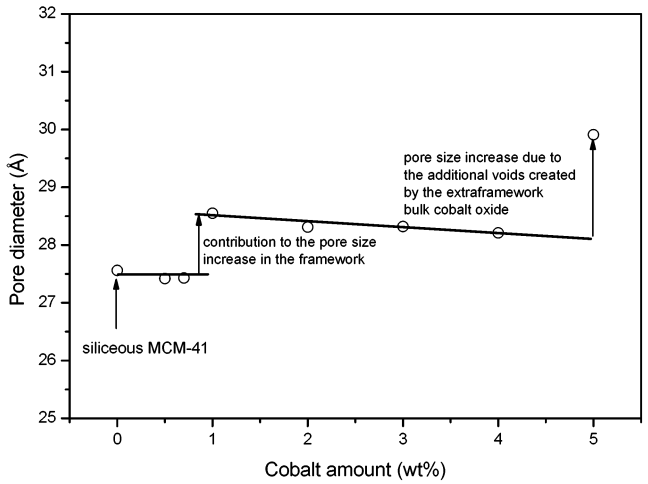

Figure 8. Pore diameter changes with the amount of cobalt incorporated.

for the sample with 5 wt % cobalt. This sample showed a bimodal pore size distribution (not shown). This sudden increase of pore size, therefore, can be attributed to the void volume of the extraframework cobalt oxide. Therefore, these results suggest the maximum amount of cobalt that can be incorporated in the MCM-41 framework is about 4 wt %. Incorporation of cobalt into the silica framework was confirmed by a TPR experiment performed between room temperature and 900 °C under 5% H_2 in argon. There was no low-temperature reduction (around 350 °C) to suggest the presence of cobalt oxide for samples containing up to 4 wt % of Co.

Different synthesis methods and materials have different crystallization times for the formation of the best MCM-41 structure. A higher synthesis temperature (150 °C) has been observed to shorten the crystallization time by enhancing the degree of condensation of silanol groups.[22] This was confirmed by XRD analysis. As discussed earlier, XRD only shows the crystalline part of the sample that has a well ordered structure. We have synthesized Co−MCM-41 samples with different crystallization times (10−192 h) at two different temperatures (100 and 150 °C). These samples were characterized by nitrogen physisorption. The slopes of the capillary condensations and fwhm values for different samples are compared in Figure 9. Pure siliceous MCM-41 shows the maximum slope and the minimum fwhm after crystallization for 4 days, whereas incorporation of cobalt required 2 more days to achieve the best

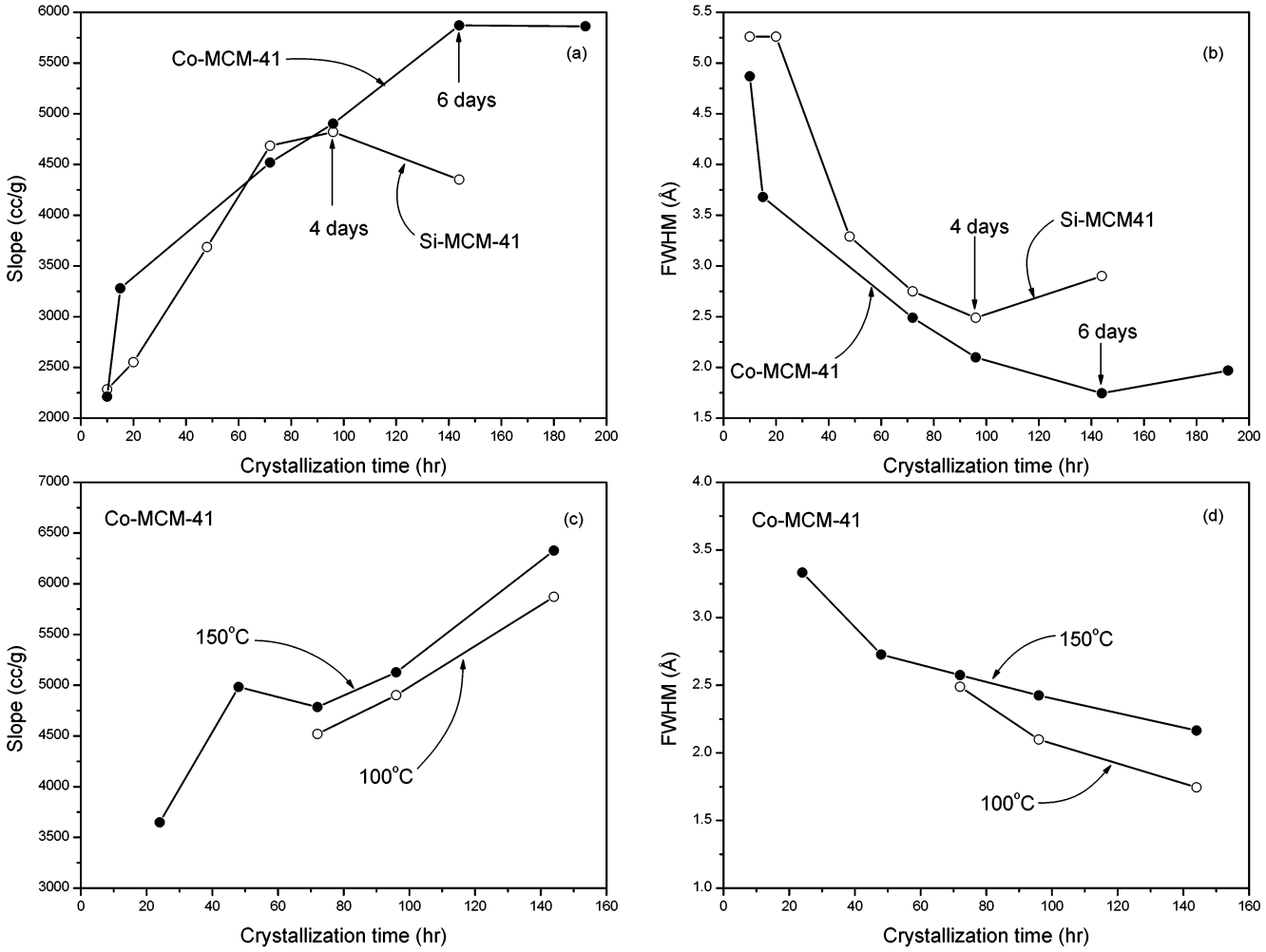

Figure 9. Optimum crystallization time and temperature of siliceous and Co−MCM-41 samples. Optimum crystallization time of Co− and Si−MCM-41 synthesized at 100 °C: (a) slope and (b) full width at half-maximum (fwhm). Preferred crystallization temperature of Co−MCM-41: (c) slope and (d) full width at half-maximum (fwhm).

structure. This may be due to the substitution of silicon by cobalt in the framework, which extends the time required for the condensation of silanol groups. The better structure of Co−MCM-41 as compared to the pure siliceous MCM-41 may be attributed to the knitting effect of cobalt as discussed above. When the crystallization temperature was 150 °C, the maximum slope increased compared to the sample synthesized at 100 °C for 6 days. The PSD curve for the sample crystallized at 150 °C, however, is broader than that of the sample crystallized at 100 °C. This suggests the sample crystallized at 150 °C contains pores of different sizes, partially collapsed pores, and incompletely formed pores. The higher temperature appears to be helpful for crystallization of the samples so that more uniform pore size distribution and regular structure could be observed, contributing to the increase of capillary condensation slope. Excessive silanol group condensation at higher temperature, however, can cause pore collapse or disorder, resulting in broad pore size distribution. From these results, the preferred crystallization temperature is 100 °C, and the optimum crystallization durations are 4 days for siliceous MCM-41 and 6 days for Co−MCM-41, respectively.

MCM-41 templates for SWNT growth must be stable under carbon deposition (reducing condition) and oxidation cycling. Figure 10 shows the XRD and XANES results of a Co−MCM-41 sample treated under various conditions to test its stability under a range of reaction conditions. The treatment conditions were as follows: reduction at 550 °C for 2 h with 5% H_2/He, reoxidation at 550 °C for 5 h under air, hydrothermal treatment at 550 °C for 5 h in an air flow saturated with water vapor, and mechanical compression in a pellet press for 3 min at ∼392 MPa (not shown). Independent of the treatment performed, all samples showed unmodified XRD and XANES patterns. The pore size distribution for each sample also remained unchanged (not shown). Finely dispersed cobalt atoms in the pore walls may maintain isolated local coordination so that they do not aggregate easily under reducing or oxidizing conditions. The optimized synthesis conditions (composition of the synthesis solution, antifoaming agent, crystallization time and temperature) may also influence the stability of the Co−MCM-41 produced. Consequently, Co−MCM-41 synthesized by the method described above is very stable at temperatures under 550 °C. Stability tests at higher temperatures are discussed in the section below.

Investigations of the C16 Co−MCM-41 Template after Carbon Deposition. The C16 Co−MCM-41 was chosen as the catalytic template for demonstrating templated growth of SWNT. The catalytic template was placed in a tubular quartz reactor of 10 mm internal diameter and heated in flowing hydrogen (150 standard cm^3/min at 1 atm) from room temperature to 500 °C at 20 °C/min. After holding the catalyst at 500 °C for 15 min, the reactor is purged with argon and then heated at 20 °C/min to 750 °C in flowing argon (150 standard cm^3/min at 4 atm).

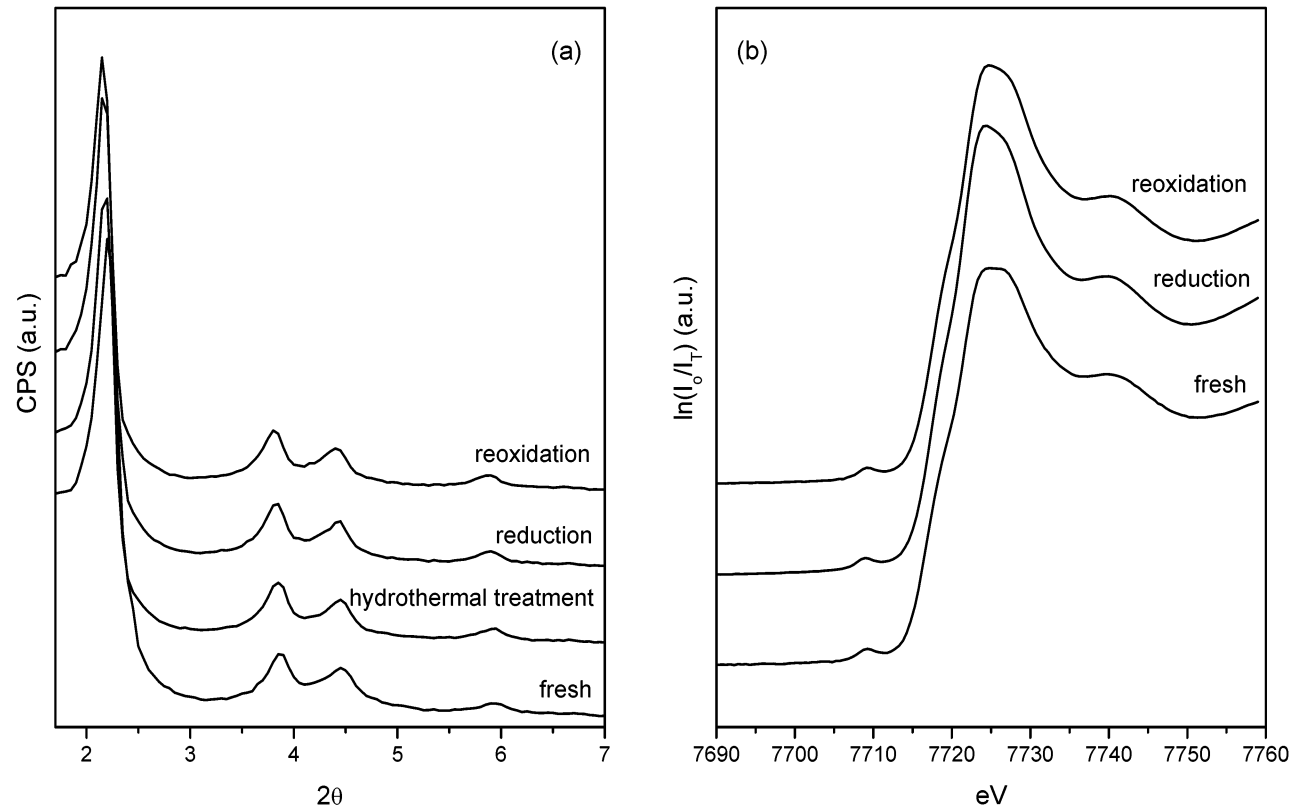

Figure 10. Stability test of Co−MCM-41 by XRD and XANES: (a) XRD patterns and (b) XANES spectra of Co−MCM-41 treated in various conditions.

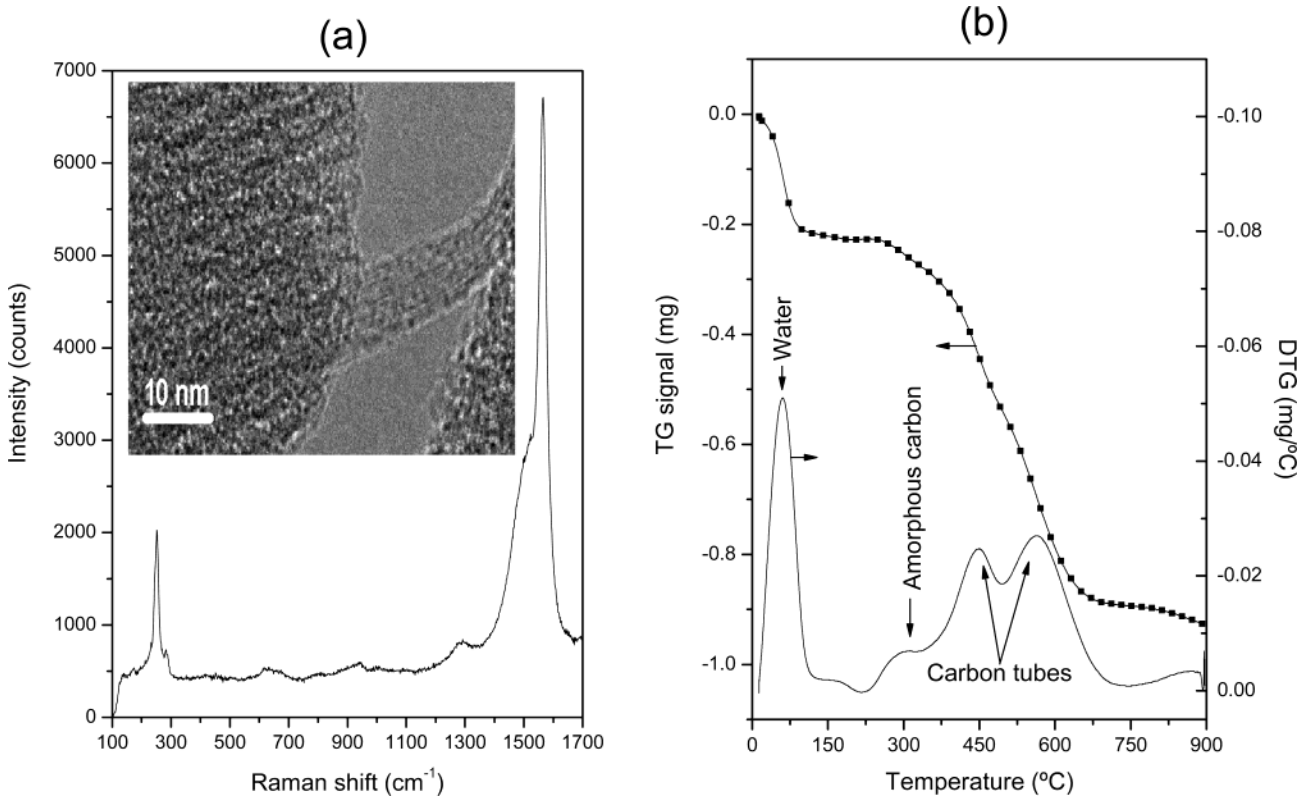

Figure 11. Raman spectrum with a TEM micrograph inset showing carbon nanotubes evolving from the pores of the MCM-41 template (a) and the TPO profile (b) recorded with an unpurified catalytic template sample after 1 h exposure to pure CO at 750 °C.

After the temperature stabilizes at 750 °C, 200 standard cm^3/min pure CO at 5 atm is fed to the reactor for 1 h. The reactor is subsequently purged with argon for 10 min at 750 °C and then cooled to room temperature in flowing argon.

Figure 11 shows the Raman spectrum with a TEM micrograph of a square area of 40 by 40 nm inset, along with the temperature programmed oxidation profile recorded for the catalytic template removed from the reactor after reaction for 1 h with pure CO,

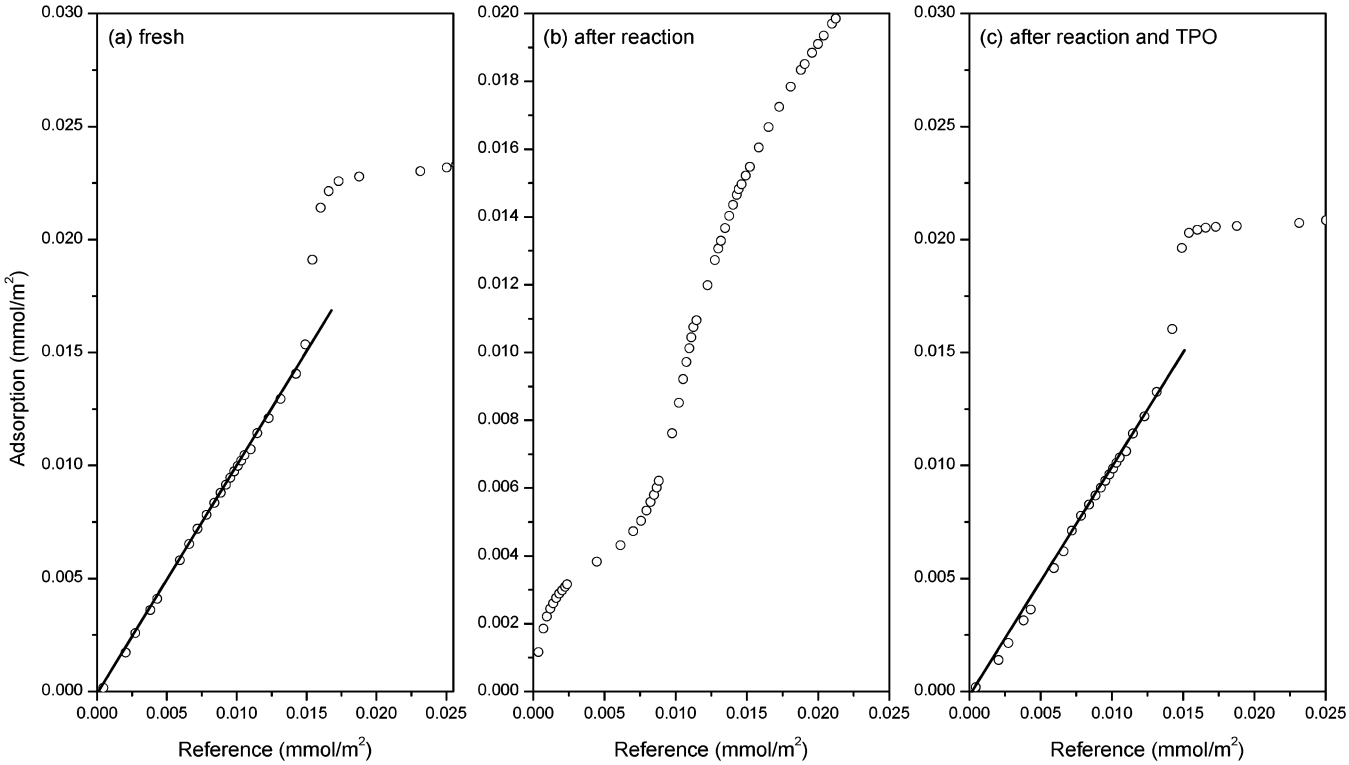

Figure 12. Comparative plot of Co−MCM-41 samples: (a) fresh; (b) after CO reaction; (c) after carbon removal.

without any other processing or purification. The TEM micrograph gives clear evidence the carbon nanotubes grow inside the pores of the catalytic template. The presence of characteristic features for the Raman breathing mode (RBM) at 253 cm^{-1} and the peak complex centered around 1580 cm^{-1} indicate the presence of single walled carbon nanotubes of narrow distribution of diameters. The tube diameter predicted from the correlations in the literature between the position of the RBM band and the tube diameter suggests the nanotubes grown in the C16 Co−MCM-41 template have an average diameter of approximately 9.2 Å. It should be noted that this spectrum was recorded with an "as prepared", unpurified sample. The low intensity of the D band centered at approximately 1300 cm^{-1}, characteristic for disordered carbon and defected carbon nanotubes, along with the TPO profile suggests a very good selectivity for SWNT synthesized using the templated method.

The presence of micropores in Co−MCM-41 templates is undesirable because the pores can be interconnected by micropores resulting in the formation of nonuniform carbon nanotubes. A comparative plot with the physisorption results was carried out for each sample to determine whether micropores are present in the catalytic templates before and after the carbon deposition, and the results are shown in Figure 12. The number of moles of adsorbate (nitrogen) per unit area of each sample was compared with that of a reference sample containing no micropores. The extrapolated linear portions of the plots recorded with the fresh template and with the catalyst exposed to CO after the carbon deposited was removed by oxidation pass through the origin, confirming the absence of micropores. However, the plot for the C16 template exposed to pure CO for 1 h indicates the presence of micropores (positive intercept on *y* axis), suggesting the micropore size of carbon nanotubes exists in the pores. The nanotube diameter determined by N_2 physisorption was about 7.5 Å. Details of this measurement are given elsewhere.[23] Taking into account an atomic radius value of 1.4 Å for carbon, this result is in good agreement

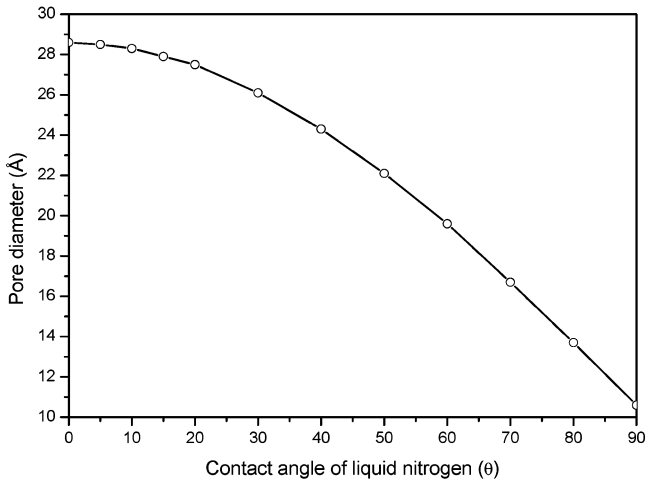

Figure 13. Pore size change with contact angle of liquid nitrogen.

with the tube diameter predicted from the Raman measurement, which considers the diameter between the centers of two carbon atoms on opposite sides of the carbon tube. The difference also could be due to the differences in the contact angle values of liquid nitrogen used in the Kelvin equation for predicting the size distribution of the micropores. The carbon nanotube internal diameter was calculated on the basis of the Kelvin equation,[24] which uses a fixed contact angle for all surfaces. When the angle was altered between 0 and 90°, the resulting diameter values dramatically changed, as shown in Figure 13. Most liquids with low surface tensions have smaller contact angles on graphite than on silica.[25] Therefore, the tube size of the nanotube may be underestimated because it was calculated with the same angle as used for template material, which is mostly silica.

For the stability test of catalytic template, a separate experiment was carried out. Prior to the growth of SWNT the sample was heated to 900 °C at a constant ramp of 10 °C/min under

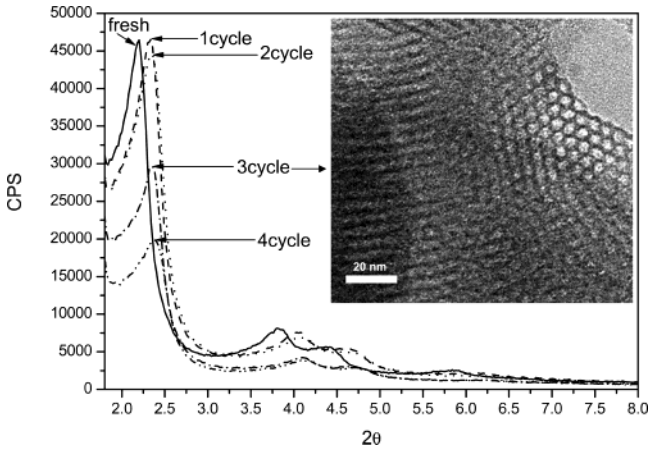

Figure 14. XRD patterns and TEM picture of Co−MCM-41 samples reacted with CO for a different number of cycles.

flowing oxygen and then cooled to 750 °C under flowing argon. After this pretreatment, the template was exposed to flowing CO for 4 h and then allowed to cool to ambient temperature under argon flow. This treatment will be further termed as one cycle. Figure 14 shows the XRD patterns of carbon deposited C16 Co−MCM-41 after each of the first through the fourth reaction cycles and the TEM picture taken after the third cycle. The catalyst structure starts to change after three cycles but still preserves its hexagonal structure even after the fourth cycle. This result shows that the Co−MCM-41 synthesized following the method described here is a highly stable catalytic template for SWNT production under harsh reaction conditions. The (100) peak is shifted to a higher angle after reaction. Assuming constant pore wall thickness, this suggests that the pore size decreases after reaction. Analysis by nitrogen physisorption (not shown) gave no evidence of serious structure collapse between reaction cycles. The pore size of the reacted samples decreased by approximately 0.3 nm compared to the fresh sample, but this may result from additional contraction and dehydroxylation due to the high-temperature treatment. However, all samples clearly showed a distinct capillary condensation and the same patterns of the adsorption/desorption isotherms. The inset TEM picture also clearly shows well maintained pore entrance and long range order of the pore side walls.

Conclusions

Highly reproducible well-ordered Co−MCM-41 samples were synthesized by a hydrothermal method with an antifoaming agent. The pore size and the mesopore volume were precisely controlled in linear dependence on the surfactant chain length. Cobalt was successfully incorporated and highly dispersed in the silica framework, which produced a Co−MCM-41 template with stable physical and chemical properties. The main cobalt species was tetrahedrally coordinated Co^{2+} in the silica framework, but the overall local environment of cobalt was a mixture of tetrahedral (Co^{2+}) and distorted tetrahedral (Co^{3+}) structures. Most of the cobalt incorporated was dispersed in the pores. Within a certain range of cobalt loadings, the structure of siliceous MCM-41 was improved by cobalt incorporation with the best structure at 1 wt % cobalt. The preferred crystallization temperature was 100 °C, and the optimum crystallization time was 4 days for siliceous MCM-41 and 6 days for Co−MCM-41, respectively. Co−MCM-41 was very stable against redox treatment up to 750 °C and maintained highly ordered structure after several reaction cycles in harsh conditions. The SWNT selectivity was over 90% with up to 4 wt % carbon loading. Formation of SWNT with highly uniform diameter was confirmed by Raman spectroscopy.

Acknowledgment. We acknowledge DARPA-DSO for the financial support of the nanotube growth and DOE-BES for the support of metal substituted MCM-41 for characterization and reactivity.

References and Notes

(1) Alvarez, W. E.; Pompeo, F.; Herrera, J. E.; Balzano, L.; Resasco, D. E. *Chem. Mater.* **2002**, *14*, 1853.
(2) Herrera, J. E.; Balzano, L.; Borgna, A.; Alvarez, W. E.; Resasco, D. E. *J. Catal.* **2001**, *204*, 129.
(3) Bronikowski, M. J.; Willis, P. A.; Colbert, D. T.; Smith, K. A.; Smalley, R. E. *J. Vac. Sci. Technol. A* **2001**, *19*, 1800.
(4) Wang, N.; Tang, Z. K.; Li, G. D.; Chen, J. S. *Nature* **2000**, *408*, 50.
(5) Tang, Z. K.; Sun, H. D.; Wang, J.; Chen, J.; Li, G. *J. Korean Phys. Soc.* **1999**, *34*, S7.
(6) Tang, Z. K.; Sun, H. D.; Wang, J.; Chen, J.; Li, G. J. *Bull. Mater. Sci.* **1999**, *22*, 329.
(7) Duxiao, J.; Nongyue, H.; Yuanying, Z.; Chunxiang, X.; Chunwei, Y.; Zuhong, L. *Mater. Chem. Phys.* **2001**, *69*, 246.
(8) Barrett, E. P.; Joyner, L. G.; Halenda, P. P. *J. Am. Chem. Soc.* **1951**, *73*, 373.
(9) Ravikovitch, P. I.; Wei, D.; Chueh, W. T.; Haller, G. L.; Neimark, A. V. *J. Phys. Chem. B* **1997**, *101*, 3671
(10) Pak, C.; Haller, G. L. *Micropor. Mesopor. Mater.* **2001**, *48*, 165.
(11) Yang, Y. H.; Lim, S.; Wang, C.; Harding, D.; Haller, G. L. *Micropor. Mesopor. Mater.*, submitted for publication.
(12) Morey, M.; Davidson, H.; Eckert, H.; Stucky, G. *Chem. Mater.* **1996**, *8*, 486.
(13) Brik, Y.; Kacimi, M.; Ziyad, M.; Verduraz, F. B. *J. Catal.* **2001**, *202*, 118.
(14) Verberckmoes, A. A.; Weckhuysen, B. M.; Schoonheydt, R. A. *Micropor. Mesopor. Mater.* **1998**, *22*, 165.
(15) Vinu, A.; D_de_ek, J.; Murugesan, V.; Hartmann, M. *Chem. Mater.* **2002**, *14*, 2433.
(16) Verberckmoes, A. A.; Uytterhoeven, M. G.; Schoonheydt, R. A. *Zeolites* **1997**, *19*, 180.
(17) Montes, C.; Davis, M. E.; Murray, B.; Narayana, M. *J. Phys. Chem.* **1990**, *94*, 6425.
(18) Mokaya, R.; Zhou, W.; Jones, W. *Chem. Commun.* **1999**, 51.
(19) Mokaya, R.; Zhou, W.; Jones, W. *J. Mater. Chem.* **2000**, *10*, 1139.
(20) Berndt, H.; Martin, A.; Zhang, Y. *Micropor. Mater.* **1996**, *6*, 1.
(21) Dzwigaj, S.; Krafft, J. M.; Che, M.; Lim, S.; Haller, G. L. *J. Phys. Chem. B* **2003**, *107*, 3856.
(22) Cheng, C. F.; Park, D. H.; Klinowski, J. *J. Chem. Soc., Faraday Trans.* **1997**, *93*, 193.
(23) Lim, S.; Ciuparu, D.;.Chen, Y.; Pfefferle, L.; Haller, G. L., to be published.
(24) Satterfield, C. T. *Heterogeneous Catalysis in Practice*; McGraw-Hill: New York, 1980.
(25) Fox, H. W.; Hare, E. F.; Zisman, W. A. *J. Phys. Chem.* **1955**, *59*, 1097.